A Nonuniform Cylindrical FDTD Algorithm with Improved PML and Quasi-PML Absorbing Boundary Conditions

Jiang-Qi He, *Student Member, IEEE,* and Qing Huo Liu, *Senior Member, IEEE*

***Abstract*— Many applications require time-domain solutions of Maxwell's equations in inhomogeneous, conductive media involving cylindrical geometries with both electrically small and large structures. The conventional finite-difference time-domain (FDTD) method with a uniform Cartesian grid will result in a staircasing error, and wastes many unnecessary cells in regions with large structures in order to accommodate the accurate geometrical representation in regions with small structures. In this work, an explicit FDTD method with a nonuniform cylindrical grid is developed for time-domain Maxwell's equations. A refined lattice is used near sharp edges and within fine geometrical details, while a larger lattice is used outside these regions. This provides an efficient use of limited computer memory and computation time. We use two absorbing boundary conditions to a nonuniform cylindrical grid: 1) the straightforward extension of Berenger's perfectly matched layer (PML) which is no longer perfectly matched for cylindrical interfaces, thus the name *quasi-PML* (QPML); 2) the improved true PML based on complex coordinates. In practice, both PML schemes can provide a satisfactory absorbing boundary condition. Numerical results are shown to compare the two absorbing boundary conditions (ABC's) and to demonstrate the effectiveness of the nonuniform grid and the absorbing boundary conditions.**

***Index Terms*—Absorbing boundary conditions, cylindrical coordinates, FDTD, nonuniform grid, numerical analysis, PML.**

I. Introduction

SIMULATIONS of transient electromagnetic waves in conductive (lossy) media have many applications such as medical imaging, nondestructive evaluation, and geophysical subsurface sensing. Finite-difference time-domain (FDTD) methods are widely applied to simulate transient electromagnetic wave propagation [1]–[4]. The predominant FDTD algorithms discretize the continuous space with a uniform Cartesian grid. In many applications, however, we have to confront the cylindrical structures such as in optical fiber communications, integrated optics, defense industry, and geophysical exploration [5], [6]. Moreover, the geometry of interest may consist of both electrically large- and small-scale structures. If we adopt the conventional FDTD method to discretize the cylindrical structure with a uniform Cartesian grid, a significant staircasing error appears. Furthermore, the cell size has to be small enough for all regions in order to accommodate the small-scale structures, wasting much computer memory and computation time. The aim of this work is to develop an FDTD algorithm with a nonuniform cylindrical grid to discretize the computational domain. Small cells are used in regions with fine details, while larger cells are used in other regions. A gradual transition is used between large and small cells.

To simulate wave propagation and scattering in an unbounded medium, absorbing boundary conditions (ABC's) have to be used to absorb outgoing waves. Many researchers, for examples Liao [7], Lindman [8], Engquist and Majda [9], Bayliss and Turkel [10], and Ramahi [11], have contributed to ABC's. However, these ABC's cannot be used for problems with oblique interfaces intersecting the outer boundary. Recently, Berenger [12], [13] introduced the perfectly matched layer (PML), which provides highly effective absorption to the outgoing waves. Chew and Weedon [14] have used the stretched coordinates to formulate the PML ABC. Katz *et al.* [15] have also validated and extended this ABC to three dimensions. Liu [16] adopts a more general stretching coordinates originally developed by Chew and Liu for elastic waves [17]–[19] to conductive media. The extension of PML to conductive media was also presented in [20] and [21]. Fang and Wu present a slightly different formulation for two dimensions [22]. Although quasi-PML (QPML) ABC formulations have been studied for nonorthogonal grids [23]–[25], only recently rigorous studies have been done on the PML for cylindrical coordinates [26]–[30].

In this work, the QPML is first formulated for cylindrical coordinates with a nonuniform grid. Although it can be shown that QPML does not give a perfect absorption [27], practically we are able to make the reflection from the QPML ABC small enough. Recently, Chew *et al.* have proposed a complex coordinate system for the development of a true PML ABC for cylindrical and spherical coordinates [28]. A FDTD method is developed for two-dimensional (2-D) polar coordinates in [29]. We improve the true PML in [28] and [29] to make it more efficient both for two and three dimensions. The concept of complex coordinates has also been used for deriving anisotropic PML [31] and for more general grid termination [32].

We first introduce in Section II a nonuniform grid in cylindrical coordinates. QPML and improved true PML ABC's in

Manuscript received February 18, 1998; revised July 6, 1998. This work was supported by the Environmental Protection Agency through a PECASE Grant CR-825-225-010, and by the National Science Foundation through a CAREER Grant ECS-9702195.

The authors are with the Klipsch School of Electrical and Computer Engineering, New Mexico State University, Las Cruces, NM 88003 USA (e-mail: qhliu@nmsu.edu).

Publisher Item Identifier S 0196-2892(99)01982-8.

0196–2892/99$10.00 © 1999 IEEE

a nonuniform grid are developed in Section III. Finally, we validate the algorithm with analytical solutions and show some applications of the nonuniform cylindrical FDTD programs in Section IV.

II. FDTD for a Nonuniform Cylindrical Grid

Consider an isotropic, inhomogeneous medium with space dependent electric permittivity $\epsilon(\boldsymbol{r})$, magnetic permeability $\mu(\boldsymbol{r})$, and conductivity $\sigma(\boldsymbol{r})$. Faraday's and Ampere's laws in Maxwell's equations are stated by

$$\nabla \times \boldsymbol{E} = -\mu \frac{\partial \boldsymbol{H}}{\partial t} - \boldsymbol{M}, \tag{1}$$

$$\nabla \times \boldsymbol{H} = \epsilon \frac{\partial \boldsymbol{E}}{\partial t} + \sigma \boldsymbol{E} + \boldsymbol{J} \tag{2}$$

where $\boldsymbol{J}$ and $\boldsymbol{M}$ are the imposed electric and magnetic current densities, respectively. The introduction of magnetic source $\boldsymbol{M}$ is convenient for modeling small loop and aperture antennas, which can be approximated as magnetic dipoles.

The FDTD solution of Maxwell's equations requires the discretization of (1) and (2). In cylindrical coordinates, (1) and (2) can be rewritten as

$$\frac{1}{\rho}\frac{\partial E_z}{\partial \phi} - \frac{\partial E_\phi}{\partial z} = -\mu \frac{\partial H_\rho}{\partial t} - M_\rho, \tag{3}$$

$$\frac{\partial E_\rho}{\partial z} - \frac{\partial E_z}{\partial \rho} = -\mu \frac{\partial H_\phi}{\partial t} - M_\phi, \tag{4}$$

$$\frac{1}{\rho}\frac{\partial(\rho E_\phi)}{\partial \rho} - \frac{1}{\rho}\frac{\partial E_\rho}{\partial \phi} = -\mu \frac{\partial H_z}{\partial t} - M_z, \tag{5}$$

$$\frac{1}{\rho}\frac{\partial H_z}{\partial \phi} - \frac{\partial H_\phi}{\partial z} = \epsilon \frac{\partial E_\rho}{\partial t} + \sigma E_\rho + J_\rho, \tag{6}$$

$$\frac{\partial H_\rho}{\partial z} - \frac{\partial H_z}{\partial \rho} = \epsilon \frac{\partial E_\phi}{\partial t} + \sigma E_\phi + J_\phi, \tag{7}$$

$$\frac{1}{\rho}\frac{\partial(\rho H_\phi)}{\partial \rho} - \frac{1}{\rho}\frac{\partial H_\rho}{\partial \phi} = \epsilon \frac{\partial E_z}{\partial t} + \sigma E_z + J_z. \tag{8}$$

As shown in Fig. 1, if we discretize the continuous space by a nonuniform cylindrical Yee grid with a variable cell size $\Delta\rho_m \times \Delta\phi_n \times \Delta z_p$, the spatial derivatives of $\boldsymbol{H}$ have to be modified from those in a uniform grid. For example, the discretized form of (6) in a nonuniform grid can be derived as

$$\begin{aligned}\frac{\epsilon}{\Delta t}&\left[E^{l}_{\rho,m+(1/2),n,p} - E^{l-1}_{\rho,m+(1/2),n,p}\right]\\ &= \frac{2}{\rho_{m+(1/2)}(\Delta\phi_{n-1}+\Delta\phi_n)}\\ &\quad\cdot\left[H^{l-(1/2)}_{z,m+(1/2),n+(1/2),p} - H^{l-(1/2)}_{z,m+(1/2),n-(1/2),p}\right]\\ &\quad - \frac{2}{(\Delta z_{p-1}+\Delta z_p)}\\ &\quad\cdot\left[H^{l-(1/2)}_{\phi,m+(1/2),n,p+(1/2)} - H^{l-(1/2)}_{\phi,m+(1/2),n,p-(1/2)}\right]\\ &\quad - \sigma E^{l-(1/2)}_{\rho,m+(1/2),n,p} - J^{l-(1/2)}_{\rho,m+(1/2),n,p}.\end{aligned} \tag{9}$$

The other two components E_ϕ, E_z can be approximated in the same way. Note that although the nonuniform grid in Fig. 1 has a variable cell size $(\Delta\rho_m \times \Delta\phi_n \times \Delta z_p)$ for the $\boldsymbol{E}$ field, the $\boldsymbol{H}$ field components are located exactly at the cell face centers. Therefore, the discretization of (3)–(5) is exactly the same as that in a uniform FDTD grid. For example, (3) can be discretized as

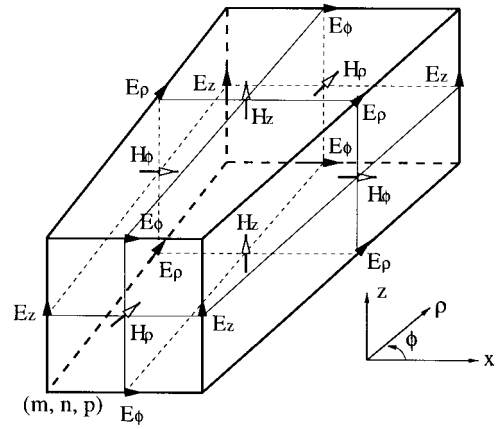

Fig. 1. A unit cell $\Delta\rho_m \times \Delta\phi_m \times \Delta z_p$ of the nonuniform cylindrical Yee grid. The $\boldsymbol{E}$ components are located at the edge centers between cells of variable sizes, while the $\boldsymbol{H}$ components are located exactly at the face centers in each cell. As a result, the FD approximated derivatives of $\boldsymbol{E}$ components at the face centers ($\boldsymbol{H}$ locations) are locally second-order accurate, while the FD approximated derivatives of $\boldsymbol{H}$ components at the edge centers ($\boldsymbol{E}$ locations) are locally first-order accurate.

$$\begin{aligned}\frac{\mu}{\Delta t}&\left[H^{l+(1/2)}_{\rho,m,n+(1/2),p+(1/2)} - H^{l-(1/2)}_{\rho,m,n+(1/2),p+(1/2)}\right]\\ &= -\frac{1}{\rho_m\cdot\Delta\phi_n}\left[E^{l}_{z,m,n+1,p+(1/2)} - E^{l}_{z,m,n,p+(1/2)}\right]\\ &\quad + \frac{1}{\Delta z_p}\left[E^{l}_{\phi,m,n+(1/2),p+1} - E^{l}_{\phi,m,n+(1/2),p}\right]\\ &\quad - M^{l}_{\rho,m,n+(1/2),p+(1/2)}.\end{aligned} \tag{10}$$

In the above equations, the time discretization is the same as in a uniform FDTD scheme.

III. Quasi-PML and Improved True PML

Since the formulation of PML in z direction in cylindrical coordinates is the same as that in Cartesian coordinates, for simplicity, we first consider Maxwell's equations in 2-D polar coordinates for the TE$_z$ case. The formulation for the TM$_z$ case can be easily derived by using duality. Here we adopt the concept of complex coordinates in [28] to present two PML formulations for polar coordinates. We use the complex coordinate stretching variables e_ρ and e_ϕ such that $(\partial/\partial\rho) \rightarrow (1/e_\rho)(\partial/\partial\rho), (\partial/\partial\phi) \rightarrow (1/e_\phi)(\partial/\partial\phi)$. In general, $e_\rho = a_\rho + i\omega_\rho/\omega$, while e_ϕ is different for the two formulations. Then, Maxwell's equations for TE$_z$ waves in a nonconductive medium in polar coordinates are modified as

$$i\omega\epsilon E_\rho = -\frac{1}{\rho e_\phi}\frac{\partial H_z}{\partial \phi}, \tag{11a}$$

$$i\omega\epsilon E_\phi = \frac{1}{e_\rho}\frac{\partial H_z}{\partial \rho}, \tag{11b}$$

$$-i\omega\mu H_z = -\frac{1}{\tilde{\rho} e_\rho}\frac{\partial(\tilde{\rho}E_\phi)}{\partial \rho} + \frac{1}{\rho e_\phi}\frac{\partial E_\rho}{\partial \phi} \tag{11c}$$

where $\tilde{\rho} = \tilde{\rho}(\rho)$ is in general a complex function that distinguishes the QPML and true PML formulations.

A. PML Scheme Using Complex Coordinates (CPML)

Choosing $e_\phi = \tilde{\rho}/\rho, e_\rho = a_\rho(\rho) + i\omega_\rho(\rho)/\omega$, and the complex radial coordinate

$$\tilde{\rho} = \int_0^\rho e_\rho(\rho')\, d\rho' = \int_0^\rho \left[a_\rho(\rho') + i\,\frac{\omega_\rho(\rho')}{\omega}\right] d\rho' = A_\rho(\rho) + i\,\frac{\Omega_\rho(\rho)}{\omega} \tag{12}$$

we rewrite (11c) as

$$i\omega\mu[H_z^{(\rho)} + H_z^{(\phi)}] = \frac{E_\phi}{\tilde{\rho}e_\rho}\,\frac{\partial\tilde{\rho}}{\partial\rho} + \frac{1}{e_\rho}\,\frac{\partial E_\phi}{\partial\rho} - \frac{1}{\tilde{\rho}}\,\frac{\partial E_\rho}{\partial\phi} \tag{13}$$

where the split field $H_z = H_z^{(\rho)} + H_z^{(\phi)}$. Then, (11a)–(11c) can be cast in the following form:

$$(-i\omega A_\rho + \Omega_\rho)\epsilon E_\rho = \frac{\partial[H_z^{(\rho)} + H_z^{(\phi)}]}{\partial\phi}, \tag{14a}$$

$$(-i\omega a_\rho + \omega_\rho)\epsilon E_\phi = -\frac{\partial[H_z^{(\rho)} + H_z^{(\phi)}]}{\partial\rho}, \tag{14b}$$

$$(-i\omega a_\rho + \omega_\rho)\mu H_z^{(\rho)} = -\frac{\partial E_\phi}{\partial\rho}, \tag{14c}$$

$$(-i\omega A_\rho + \Omega_\rho)\mu H_z^{(\phi)} = -E_\phi + \frac{\partial E_\rho}{\partial\phi}. \tag{14d}$$

Equations (14a)–(14d) can be easily transformed to time domain.

Based on this scheme, the set of time-domain equations for updating $\boldsymbol{E}$ field for conductive media in three-dimensional (3-D) cylindrical coordinates are

$$A_\rho\epsilon\,\frac{\partial E_\rho^{(\phi)}}{\partial t} + (\Omega_\rho\epsilon + A_\rho\sigma)E_\rho^{(\phi)} + \Omega_\rho\sigma\int_{-\infty}^t E_\rho^{(\phi)}(\tau)\,d\tau = \frac{\partial H_z}{\partial\phi} - \rho J_\rho^{(\phi)}, \tag{15a}$$

$$a_z\epsilon\,\frac{\partial E_\rho^{(z)}}{\partial t} + (\omega_z\epsilon + a_z\sigma)E_\rho^{(z)} + \omega_z\sigma\int_{-\infty}^t E_\rho^{(z)}(\tau)\,d\tau = -\frac{\partial H_\phi}{\partial z} - J_\rho^{(z)}, \tag{15b}$$

$$a_\rho\epsilon\,\frac{\partial E_\phi^{(\rho)}}{\partial t} + (\omega_\rho\epsilon + a_\rho\sigma)E_\phi^{(\rho)} + \omega_\rho\sigma\int_{-\infty}^t E_\phi^{(\rho)}(\tau)\,d\tau = -\frac{\partial H_z}{\partial\rho} - J_\phi^{(\rho)}, \tag{15c}$$

$$a_z\epsilon\,\frac{\partial E_\phi^{(z)}}{\partial t} + (\omega_z\epsilon + a_z\sigma)E_\phi^{(z)} + \omega_z\sigma\int_{-\infty}^t E_\phi^{(z)}(\tau)\,d\tau = \frac{\partial H_\rho}{\partial z} - J_\phi^{(z)}, \tag{15d}$$

$$a_\rho\epsilon\,\frac{\partial E_z^{(\rho)}}{\partial t} + (\omega_\rho\epsilon + a_\rho\sigma)E_z^{(\rho)} + \omega_\rho\sigma\int_{-\infty}^t E_z^{(\rho)}(\tau)\,d\tau = \frac{\partial H_\phi}{\partial\rho} - J_z^{(\rho)}, \tag{15e}$$

$$A_\rho\epsilon\,\frac{\partial E_z^{(\phi)}}{\partial t} + (\Omega_\rho\epsilon + A_\rho\sigma)E_z^{(\phi)} + \Omega_\rho\sigma\int_{-\infty}^t E_z^{(\phi)}(\tau)\,d\tau = H_\phi - \frac{\partial H_\rho}{\partial\phi} - \rho J_z^{(\phi)}. \tag{15f}$$

The other set of equations for updating $\boldsymbol{H}$ can be obtained by duality. The set of (15) are appropriate for time-stepping. Compared with the formulations in [29], for nonconductive media this system requires 12 instead of 16 field variables, saving about 33% computer memory. This scheme also provides additional degree of freedom (a_ρ and A_ρ) for the PML.

B. QPML Scheme

Note that in the unified formula (11a)–(11c), if we choose $e_\phi = e_\rho = a_\rho(\rho) + i\omega_\rho(\rho)/\omega$, and $\tilde{\rho}(\rho) = \rho$, we can rewrite the 3-D updating equations for $\boldsymbol{E}$ field in time-domain for conductive media as

$$a_\rho\epsilon\,\frac{\partial E_\rho^{(\phi)}}{\partial t} + (\omega_\rho\epsilon + a_\rho\sigma)E_\rho^{(\phi)} + \omega_\rho\sigma\int_{-\infty}^t E_\rho^{(\phi)}(\tau)\,d\tau = \frac{1}{\rho}\,\frac{\partial H_z}{\partial\phi} - J_\rho^{(\phi)}, \tag{16a}$$

$$a_z\epsilon\,\frac{\partial E_\rho^{(z)}}{\partial t} + (\omega_z\epsilon + a_z\sigma)E_\rho^{(z)} + \omega_z\sigma\int_{-\infty}^t E_\rho^{(z)}(\tau)\,d\tau = -\frac{\partial H_\phi}{\partial z} - J_\rho^{(z)}, \tag{16b}$$

$$a_\rho\epsilon\,\frac{\partial E_\phi^{(\rho)}}{\partial t} + (\omega_\rho\epsilon + a_\rho\sigma)E_\phi^{(\rho)} + \omega_\rho\sigma\int_{-\infty}^t E_\phi^{(\rho)}(\tau)\,d\tau = -\frac{\partial H_z}{\partial\rho} - J_\phi^{(\rho)}, \tag{16c}$$

$$a_z\epsilon\,\frac{\partial E_\phi^{(z)}}{\partial t} + (\omega_z\epsilon + a_z\sigma)E_\phi^{(z)} + \omega_z\sigma\int_{-\infty}^t E_\phi^{(z)}(\tau)\,d\tau = \frac{\partial H_\rho}{\partial z} - J_\phi^{(z)}, \tag{16d}$$

$$a_\rho\epsilon\,\frac{\partial E_z}{\partial t} + (\omega_\rho\epsilon + a_\rho\sigma)E_z + \omega_\rho\sigma\int_{-\infty}^t E_z(\tau)\,d\tau = \frac{1}{\rho}\,\frac{\partial(\rho H_\phi)}{\partial\rho} - \frac{1}{\rho}\,\frac{\partial E_\rho}{\partial\phi}\,J_z. \tag{16e}$$

Therefore, there are only ten field variables in the 3-D QPML formulation. Although it can be shown theoretically that this PML is not perfectly matched (thus the name *quasi*-PML) [27], practically it provides a satisfactory ABC with a 20% saving in computer memory and computation time compared with the improved true PML (CPML) scheme.

C. Discretization of Time-Domain Equations

We adopt the modified Yee's algorithm in Section II to discretize the above equations in a nonuniform grid. As an example, (16a) in the time-stepping form becomes

$$\begin{aligned} E_\rho^{(\phi)}(i,j,k,n+1) &= f_1(i,j,k)E_\rho^{(\phi)}(i,j,k,n) + f_2(i,j,k)E_{I\rho}^{(\phi)}(i,j,k,n) \\ &\quad + f_3(i,j,k)[H_z(i,j,k,n) - H_z(i,j-1,k,n)] \\ &\quad + f_4(i,j,k)J_\rho^{(\phi)}(i,j,k,n) \end{aligned} \tag{17}$$

where

$$f_1(i,j,k) = \frac{a_\rho\epsilon/\Delta t - (a_\rho\sigma + \omega_\rho\epsilon)/2}{a_\rho\epsilon/\Delta t + (a_\rho\sigma + \omega_\rho\epsilon + \omega_\rho\sigma\Delta t)/2}, \tag{18a}$$

$$f_2(i,j,k) = \frac{-\omega_\rho \sigma \Delta t}{a_\rho \epsilon/\Delta t + (a_\rho \sigma + \omega_\rho \epsilon + \omega_\rho \sigma \Delta t)/2}, \tag{18b}$$

$$f_3(i,j,k) = \frac{2/(\Delta\phi_{j-1} + \Delta\phi_j)}{\rho_{m+1/2}[a_\rho \epsilon/\Delta t + (a_\rho \sigma + \omega_\rho \epsilon + \omega_\rho \sigma \Delta t)/2]}, \tag{18c}$$

$$f_4(i,j,k) = -\frac{\Delta t}{\epsilon + \sigma \Delta t/2}. \tag{18d}$$

In (18), parameters ϵ, μ, σ are all functions of space for an inhomogeneous medium. Note that the time-integrated electric field $E_{I\rho}^{(\phi)}$ is located at the same position in the staggered grid as the electric field $E_\rho^{(\phi)}$. Moreover, terms involving $\boldsymbol{E}$ at $t = (n + (1/2))\Delta t$ and $\boldsymbol{H}$ at $t = n\Delta t$ require time interpolation (averaging) as they are not defined at these discrete points. This averaging has the same accuracy as the central time differencing, and therefore does not degrade the overall accuracy in the time discretization. Similar expressions can be derived for the other field components.

The QPML is not completely reflectionless. However, its simplicity, less computer memory and computational time, and reasonably small reflections make it attractive to many applications. In comparison, the improved true PML is reflectionless in the continuous limit, but requires additional memory and computation time. In practice, our results show little reflection from both the true PML and QPML interfaces.

IV. Numerical Results

We have implemented the FDTD algorithm with both ABC's for 2-D axisymmetric, 2-D polar, and 3-D cylindrical problems. To minimize the reflection from the discretized PML layers, we choose a quadratic profile for the PML coordinate-stretching variables whose maximum values are denoted by $a_{\eta,\max}$ and $\omega_{\eta,\max}$ $(\eta = \rho, z)$ at the outer boundaries. Numerical results are shown below to demonstrate the applications of the FDTD algorithm. In the following examples, a magnetic or an electric dipole directed in the z direction is used as a source, and the field component H_z is measured at an array of receivers. The source time function is the first derivative of the Blackman–Harris window function with a center frequency of f_c. Unlike the previous ABC's, the PML ABC's in this FDTD algorithm are stable even after 60 000 time steps.

A. Order of Accuracy

It has been demonstrated [33], [34] that the nonuniform Cartesian grid FDTD is locally first-order accurate, but globally second-order accurate (known as *supraconvergence*). Although the analysis in [33] and [34] cannot be easily applied to cylindrical coordinates, we can numerically show the order of accuracy in the nonuniform cylindrical FDTD scheme. We design an experiment for testing the error as a function of the cell size $(\Delta\rho, \Delta\phi)$ in polar coordinates for a homogeneous medium with perfect electric conductor as the outer boundary. We fix locations of the source and receiver as well as the physical size of the computation region. The computational region is discretized by a grid of $N_\rho \times N_\phi$ (where $N_\rho = N_\phi$) cells with a random distribution of $\Delta\rho$ and $\Delta\phi$. We gradually decrease the number $N_\rho = N_\phi$, i.e., we increase the average cell size, from the reference model which has a very fine grid. Within a fixed time period, we calculated the global error for each experiment with respect to the reference case. Fig. 2 shows the error as a function of $1/N_\rho$ which clearly confirms the supraconvergence of second-order accuracy of the FDTD scheme.

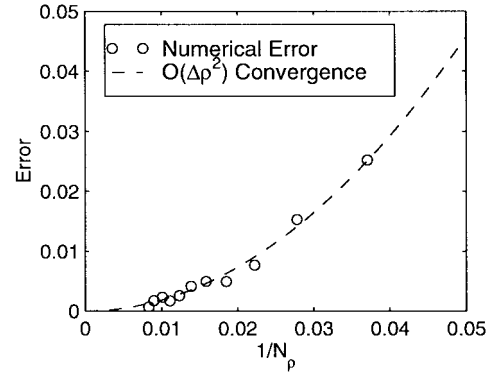

Fig. 2. Error of the nonuniform cylindrical FDTD scheme as a function of the $1/N_\rho$ showing the $O(\Delta\rho^2)$ convergence. The number N_ϕ increases proportionally with N_ρ.

B. A Conductive Sphere in a Nonconductive Medium with QPML

This special case is to model a conductive sphere in a nonconductive background medium with a z-directed magnetic dipole ring source ($f_c = 100$ MHz) at the center of the sphere. This is a 2-D axisymmetric case. The conductive sphere has a radius of 0.7 m with $\epsilon_r = 4, \mu_r = 1$, and $\sigma = 10^{-4}$ S/m. Outside the sphere is a nonconductive medium with $\epsilon_r = 1, \mu_r = 1$, and $\sigma = 0$. For the boundary condition, we use 10 cells of QPML in z direction and 20 cells in ρ direction. The size of the computational domain is $N_\rho \times N_z = 80 \times 140$ and the nonuniform cell size (in meters) has the profile $\Delta\rho_m = 0.03 + 0.0005\, m$ in ρ direction and $\Delta z_p = 0.03 + 0.0005|p - 70|$ in z direction. The source is located at the sphere center and at cell $(i_\rho, i_z) = (0, 70)$, and the receiver is located at cell (0, 80). Fig. 3 compares the QPML result with the analytical solution for the received H_z waveform. The small error shown in the inset is caused by three major sources: the PML reflection, the staircasing error of the sphere model, and the approximation of the small ring source by a point source in the analytical solution.

C. A Polar Case in Free Space with QPML and CPML

In this case, we simulate a line magnetic current source M_z in free space with a center frequency $f_c = 300$ MHz. This is a 2-D polar problem (TE$_z$ waves). The line source is located at the cell $(i_\rho, i_\phi) = (15, 64)$ in a cylindrical domain of $N_\rho \times N_\phi = 80 \times 256$ cells ($\rho_{\max} = 3.2$ m) including 10 PML cells in the radial direction. Fig. 4 shows the excellent agreement between analytical solution and the numerical results of the QPML and CPML schemes for a receiver at cell (20, 72). The reflection is about 1.1% and 0.91% for QPML and CPML, respectively. Note that for a fair

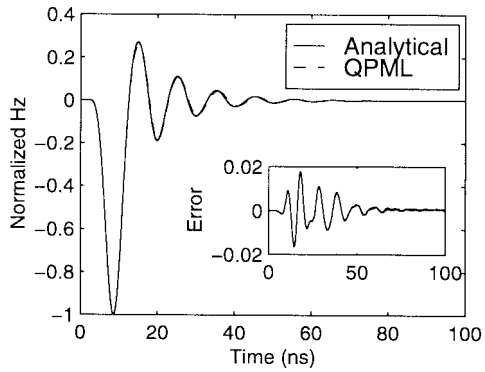

Fig. 3. The H_z component at a receiver near a conductive sphere (radius 0.7 m, $\epsilon_r = 4, \mu_r = 1$, and $\sigma = 10^{-4}$ S/m) in a nonconductive background medium ($\epsilon_r = 1, \mu_r = 1$, and $\sigma = 0$). A small magnetic ring source is located at the center of the sphere. The inset shows the difference between the numerical and analytical results.

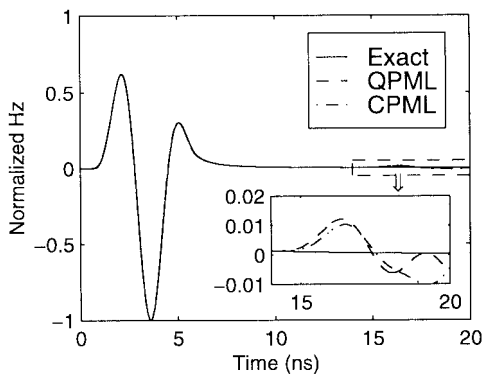

Fig. 4. Comparison between analytical and numerical results for the QPML and true CPML schemes for a free space in polar coordinates. The computational domain is $N_\rho \times N_\phi = 80 \times 256$. The line source is located at the cell $(j_\rho, j_\phi) = (15, 64)$.

comparison, we have chosen $a_\rho = 1$ in the QPML case even though the code allows a profile for a_ρ. As discussed below, this reflection can be reduced substantially by adjusting a_ρ. It is worthwhile to point out that, as the radius of the truncating boundary increases, the difference between the QPML and CPML diminishes [27].

D. Effect of a_ρ in the QPML ABC

In the above examples, we observe that in cylindrical coordinates, there is some small reflection in the ρ direction from the boundary, and this reflection increases with the incidence angle. We found that the reflection can be reduced by the appropriate choice of PML parameters ω_ρ and a_ρ. We first choose an optimal ω_ρ, then adjust a_ρ to achieve further reduction to the reflection. Here, we show the effects of a_ρ on the reflected field.

To quantify the QPML reflection, we simulate two axisymmetric problems with grid sizes $N_\rho \times N_z = 290 \times 140$ and $N_\rho \times N_z = 80 \times 140$. The source ($f_c = 100$ MHz) and the receiver are located at (0, 30) and (59, 40), respectively. In the geometry of the smaller grid, the incident angle is approximately 10° at the receiver location. The incident and total fields are obtained from the larger grid and the smaller

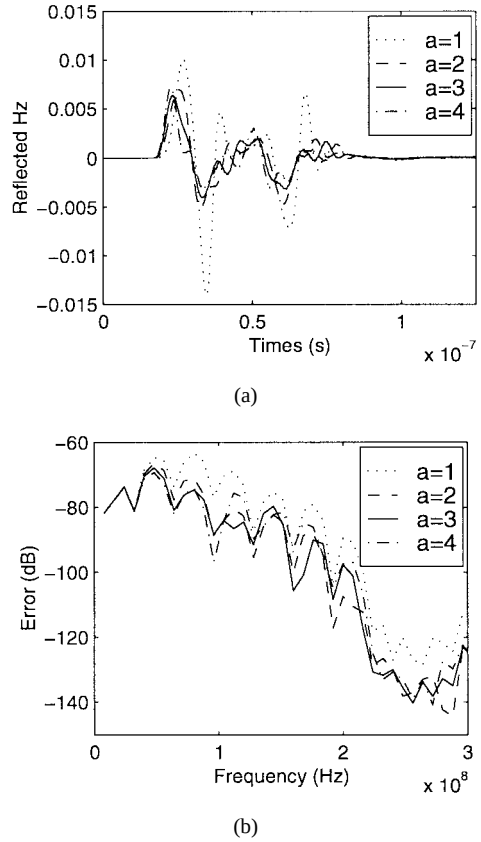

Fig. 5. Reflected fields for $a_{\rho,\max} = 1, 2, 3$, and 4 in an axisymmetric problem. (a) Time-domain reflected field H_z^R. (b) Spectral amplitude of the reflected field normalized by the peak spectral amplitude of the incident field.

grid, respectively. The difference of these two fields gives the reflected field from the boundary. Fig. 5(a) and (b) show the reflected waveforms and their spectral amplitudes for four different values of $a_{\rho,\max} = 1$, 2, 3, and 4. Corresponding to the reflected waveforms H_z^R in Fig. 5(a), the L_∞ errors $E_\infty = \max\{|H_z^R(t_j)|, j = 0, \cdots N_t\}$ are 0.0140, 0.006 94, 0.006 35, and 0.007 21, respectively; while the L_2 errors $E_2 = \sqrt{\Sigma_{j=0}^{N_t} |H_z^R(t_j)|^2}$ are 0.1685, 0.0989, 0.0816, and 0.0774, respectively. As it is preferable to choose the value of $a_{\rho,\max}$ which gives the smallest L_∞ error, the value of $a_{\rho,\max} = 3$ is more desirable, even though it has a slightly larger L_2 error than $a_{\rho,\max} = 4$. The spectral amplitude in Fig. 5(b) shows that the reduction in the reflected field for $a_{\rho,\max} > 1$ is broadband.

E. An Application of the Nonuniform Cylindrical FDTD Method

We model a 3-D case to illustrate the application of the nonuniform cylindrical FDTD using PML ABC's. Fig. 6(a) shows the xz cross section of a 3-D borehole radar detection problem with vertical and horizontal fractures. The background medium is conductive with $\epsilon_r = 2, \mu_r = 1$, and $\sigma = 0.001$ S/m. The centered borehole has a radius of 16 cm and $\epsilon_r = 4, \mu_r = 1$, and $\sigma = 0.01$ S/m. The horizontal fracture has a thickness of 3 cm with $\epsilon_r = 8, \mu_r = 1$, and $\sigma = 0.1$ S/m. A vertical fracture is located about 1.73 m away from the borehole axis. It has a thickness of 3 cm and spans 9° in ϕ

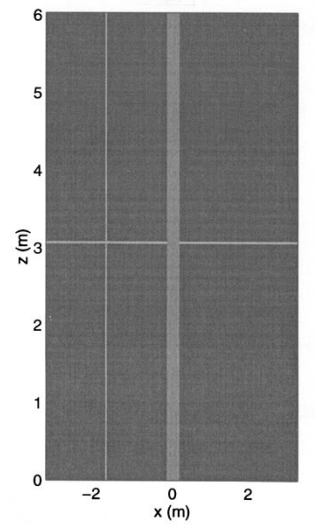

(a)

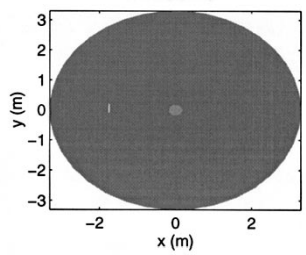

(b)

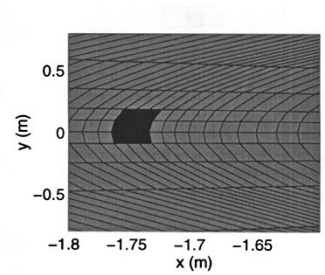

(c)

Fig. 6. Detection of horizontal and vertical fractures by a borehole radar in a borehole radius 16 cm. The thickness of fractures is 3 cm. (a) The xz cross section. (b) The xy cross section. (c) Part of the magnified cells in (b) around the vertical fracture.

direction, and has the same ϵ_r, μ_r, and σ as the horizontal fracture. Fig. 6(b) shows the xy cross section which is further magnified in Fig. 6(c) to show the grid around the vertical fracture. A magnetic dipole point source is located along the borehole axis and is 3.8 m from the bottom boundary, and an array of receivers is also located along the borehole axis. If this problem were to be simulated by a uniform FDTD code, a grid about $N_\rho \times N_\phi \times N_z = 600 \times 120 \times 350$ should have been used in order to accommodate the small fractures in different directions. Here, we adopt a nonuniform grid with $N_\rho \times N_\phi \times N_z = 140 \times 40 \times 100$, saving about 45 times CPU and memory.

The scattered field due to both fractures is shown in Fig. 7. Because the horizontal fracture is much larger, the scattered field is dominated by that from this fracture. As a result the scattered field waveforms show a symmetric pattern centered at the location of the horizontal fracture. The scattering due to the vertical fracture can be obtained by subtracting the contribution of the horizontal fracture from the total scattered field. Quantitative analysis shows that the vertical fracture contributes only about 1/60 of the scattered field in Fig. 7.

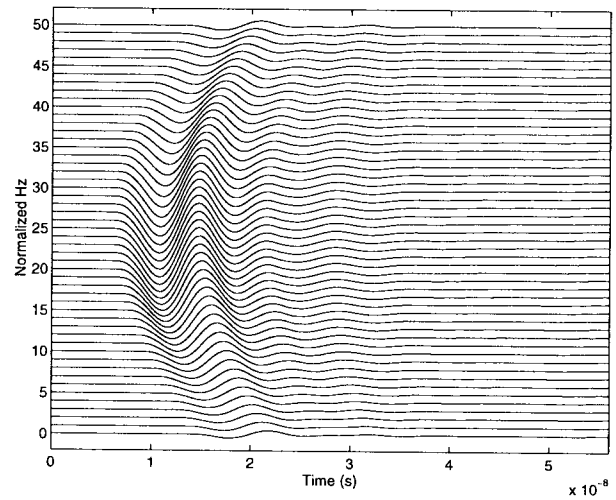

Fig. 7. Waveforms of the scattered field from the two fractures in Fig. 6. The field is normalized by one-fifth of the maximum peak value.

V. Conclusions

We have developed an FDTD algorithm with a nonuniform cylindrical grid. The QPML and improved true PML absorbing boundary conditions are extended to a nonuniform grid. The FDTD algorithm with PML ABC's is validated by analytical solutions to canonical problems. Unlike the previous ABC's, the PML absorbing boundary conditions have long-time stability even when an oblique interface intersects the truncating boundary. This algorithm with a nonuniform cylindrical grid is more flexible for problems with varying scales of geometry and can greatly save computer memory and computation time. The QPML algorithm requires less computer memory and computation time, while the true PML gives slightly smaller reflections.

Acknowledgment

The authors would like to thank W. C. Chew for some useful discussions, and the reviewers for their constructive criticisms to improve the quality of the manuscript.

References

[1] K. S. Yee, "Numerical solution of initial boundary value problems involving Maxwell's equations in isotropic media," *IEEE Trans. Antennas Propagat.*, vol. 14, pp. 302–307, 1966.
[2] K. S. Kunz, and R. J. Luebbers, *Finite Difference Time Domain Method for Electromagnetics*. Florida: CRC, 1993.
[3] W. C. Chew, *Waves and Fields in Inhomogeneous Media*. Piscataway, NJ: IEEE Press, 1995.
[4] A. Taflove, *Computational Electrodynamics: The Finite Difference Time Domain Method*. Boston, MA: Artech House, 1995.

[5] Q. H. Liu, "Diffraction of nonaxisymmetric waves in cylindrically layered media by horizontal discontinuities," *Radio Sci.*, vol. 27, pp. 569–581, 1992.
[6] ——, "Electromagnetic field generated by an off-axis source in a cylindrically layered medium with an arbitrary number of horizontal discontinuities," *Geophys.*, vol. 58, pp. 616–625, 1993.
[7] Z. P. Liao, H. L. Wong, B. P. Yang, and Y. F. Yuan, "A transmitting boundary for transient wave analysis," *Sci. Sinica A*, vol. 27, pp. 1063–1076, 1984.
[8] E. L. Lindman, "Free space boundary conditions for the time dependent wave equation," *J. Comput. Phys.*, vol. 18, pp. 66–78, 1975.
[9] B. Engquist and A. Majda, "Absorbing boundary conditions for the numerical simulation of waves," *Math. Comput.*, vol. 31, pp. 629–51, 1977.
[10] A. Bayliss and E. Turkel, "Radiation boundary conditions for wavelike equations," *Commun. Pure Appl. Math.*, vol. 33, pp. 707–25, 1980.
[11] O. M. Ramahi, "Complementary operator: A method to annihilate artificial reflections arising from the truncation of the computational domain in the partial differential equations," *IEEE Trans. Antennas Propagat.*, vol. AP-43, pp. 697–704, 1995.
[12] J.-P. Berenger, "A perfectly matched layer for the absorption of electromagnetic waves," *J. Comput. Phys.*, vol. 114, pp. 185–200, 1994.
[13] ——, "Three-dimensional perfectly matched layer for the absorption of electromagnetic waves," *J. Comput. Phys.*, vol. 127, pp. 363–379, 1996.
[14] W. C. Chew, and W. H. Weedon, "A 3D perfectly matched medium from modified Maxwell's equations with stretched coordinates," *Microwave Opt. Tech. Lett.*, vol. 7, pp. 599–604, 1994.
[15] D. S. Katz, E. T. Thiele, and A. Taflove, "A perfectly matched layer for the absorbing of electromagnetic waves," *IEEE Microwave Guided Wave Lett.*, vol. 4, pp. 268–270, 1994.
[16] Q. H. Liu, "An FDTD algorithm with perfectly matched layers for conductive media," *Microwave Opt. Tech. Lett.*, vol. 14, pp. 134–137, 1997.
[17] W. C. Chew, and Q. H. Liu, "Perfectly matched layers for elastodynamics: A new absorbing boundary condition," Schlumberger-Doll Res. Tech. Rep., Aug. 1995.
[18] ——, "Using perfectly matched layers for elastodynamics," in *Proc. IEEE Antennas and Propagation Soc. Int. Symp.*. New York, 1996, vol. 1, pp. 366–369.
[19] ——, "Perfectly matched layers for elastodynamics: A new absorbing boundary condition," *J. Comput. Acoust.*, vol. 4, pp. 72–79, 1996.
[20] Q. H. Liu, "A spectral-domain method with perfectly matched layers for time-domain solutions of Maxwell's equations," in *Proc. 1996 URSI Meet.*, Baltimore, MD, July 1996.
[21] Y. H. Chen, W. C. Chew, and M. Oristaglio, "Elongated 3D FDTD Modeling using PML," in *1996 Int. IEEE AP-S Symp. Dig.*, Baltimore, MD, July 1996.
[22] J. Fang and Z. Wu, "Generalized perfectly matched layer an extension of Berenger's perfectly matched layer boundary condition," *IEEE Microwave Guided Waves Lett.*, vol. 5, pp. 451–453, 1995.
[23] E. A. Navarro, C. Wu, P. Chung, and J. Litva, "Application of PML superabsorbing boundary condition to nonorthogonal FDTD method," *Electron. Lett.*, vol. 30, pp. 1654–1656, 1994.
[24] W. Chen, E. A. Navarro, P. Y. Chung, and J. Litva, "Modeling of waveguide structures using the nonorthogonal FDTD method with a PML Absorbing boundary," *Microwave Opt. Tech. Lett.*, vol. 8, pp. 226–228, 1995.
[25] J. A. Roden and S. D. Gedney, "Efficient implementation of the uniaxial-based PML media in three-dimensional nonorthogonal coordinates with the use of FDTD technique," *Microwave Opt. Tech. Lett.*, vol. 14, pp. 71–75, 1997.
[26] J. Maloney, M. Kesler, and G. Smith, "Generalization of PML to cylindrical geometries," in *Proc. 13th Annual Review of Progress in Applied Computational Electromagnetics*, Monterey, CA, Mar. 1997.
[27] Q. H. Liu and J. Q. He, "Quasi-PML for waves in cylindrical coordinates," New Mexico State Univ. Tech. Rep., July 1997. Also to appear in *Microwave Opt. Tech. Lett.*, vol. 19, pp. 107–111, Oct. 1998.
[28] W. C. Chew, J. M. Jin, and E. Michelssen, "Complex coordinate system as a generalized absorbing boundary condition," *Microwave Opt. Tech. Lett.*, vol. 15, pp. 363–369, 1997.
[29] F. L. Teixeira and W. C. Chew, "PML-FDTD in cylindrical and spherical grids," *IEEE Microwave Guided Wave Lett.*, vol. 7, pp. 285–287, 1997.
[30] B. Yang, D. Gottlieb, and J. S. Hesthaven, "Spectral simulations of electromagnetic wave scattering," *J. Comput. Phys.*, vol. 134, pp. 216–230, 1997.
[31] F. L. Teixeira, and W. C. Chew, "Systematic derivation of anisotropic PML absorbing media in cylindrical and spherical coordinates," *IEEE Microwave Guided Wave Lett.*, vol. 7, pp. 371–373, 1997.
[32] F. L. Teixeira, and W. C. Chew, "Analytical derivation of a conformal perfectly matched absorber for electromagnetic waves," *Microwave Opt. Tech. Lett.*, vol. 17, pp. 231–236, 1998.
[33] P. Monk and E. Suli, "A convergence analysis of Yee's scheme on nonuniform grids," *SIAM J. Numer. Anal.*, vol. 31, pp. 393–412, 1994.
[34] P. Monk, "Error estimates for Yee's method on nonuniform grids," *IEEE Trans. Magnet.*, vol. 30, pp. 3200–3203, 1994.

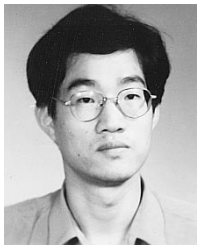

Jiang-Qi He (S'97) received the B.S. degree in physics from Xiamen University, China, in 1992, and the M.S. degree in electrical engineering from New Mexico State University, Las Cruces, in 1997.

Since May 1996, he has been a Research Assistant in Electromagnetic Laboratory, Klipsch School of Electrical and Computer Engineering, New Mexico State University. His current research interests include computational electromagnetics and numerical methods.

Qing Huo Liu (S'88–M'89–SM'94), for a photograph and biography, see this issue, p. 926.